# Mesoscale eddy modulation of subsurface chlorophyll maximum layers in the South China Sea

Wenlong Xu[1,2,3], Guifen Wang[1, 2, *], Xuhua Cheng[1,2], Xiaogang Xing[4], Jianhuang Qin[1,2], Guidi Zhou[1,2], Long Jiang[1,2], Bingzhang Chen[5]

1. Key Laboratory of Marine Hazards Forecasting, Ministry of Natural Resources, Hohai University, Nanjing, China

2. College of Oceanography, Hohai University, Nanjing, China

3. Ocean College, Jiangsu University of Science and Technology, Zhenjiang, China

4. State Key Laboratory of Satellite Ocean Environment Dynamics, Second Institute of Oceanography, Ministry of Natural Resources, Hangzhou, China

5. Department of Mathematics and Statistics, University of Strathclyde, Glasgow, United Kingdom

*Corresponding author: Guifen Wang (guifenwang@hhu.edu.cn)

**Key points:**

(1) Anticyclonic (cyclonic) eddies support deeper (shallower), thicker (thinner), and weaker (stronger) SCM layers.

(2) The impact of eddy on SCM characteristics is the strongest near the eddy center and increases with the eddy amplitude.

(3) The diatoms in SCM layer increased in cyclonic eddies, while more coccolithophores are found in anticyclonic eddies.

Mesoscale eddy modulation of subsurface chlorophyll maximum layers in the South China Sea

## Abstract

Subsurface chlorophyll maximum (SCM) layers contribute considerably to the integrated biomass of the water column and can be strongly modulated by mesoscale eddies that are ubiquitous in the global ocean. The mechanisms of eddy-induced surface chlorophyll concentration have been extensively examined in the South China Sea (SCS). However, the potential impact of mesoscale eddies on SCM layers remains unclear. We examined the influence of mesoscale eddies on the depth, thickness and magnitude of SCM layers in the SCS using output from an eddy-permitting biological–physical coupled model over a 22-year period. Our study shows that nutrient distribution is largely driven by eddy dynamics, with cyclonic eddies enhancing the supply of inorganic nutrients in the upper layers by uplifting the thermocline, and downward displacement of the thermocline in anticyclonic eddies, reducing the nutrient supply into the euphotic zone from the depth. We found that anticyclonic (cyclonic) eddies are responsible for increased (decreased) SCM depth and decreased (increased) SCM magnitude; SCM thickness decreased in cyclonic eddies but slightly increased in anticyclonic eddies. The effects of mesoscale eddies depend on eddy amplitude. Maximal anomalies in depth, thickness and magnitude always occur near the center of eddies. Phytoplankton community structure at SCM layers is also affected by eddies, with more diatoms in cyclonic eddies and more coccolithophores in anticyclonic eddies. Our study will advance our understanding of mesoscale physical–biogeochemical interactions.

**Plain Language Summary**

Mesoscale eddies, which are ubiquitous features in the global ocean, play an important role in ocean circulation and dynamics and have profound effects on the biogeochemical cycles. We investigate how these eddies control the characteristics of the subsurface chlorophyll maximum (SCM) layer (including SCM depth, thickness and magnitude) in the South China Sea. Anticyclonic (cyclonic) eddies increase (reduce) SCM depth and decrease (increase) SCM magnitude; SCM thickness decreases in cyclonic eddies and increases slightly in anticyclonic eddies. The effect of eddies on the phytoplankton community structure in the surface layer was different from that in the subsurface layer, altering the proportion of pico-prokaryotes at the surface and the percentage of diatom and coccolithophores at the subsurface. The largest anomalies in SCM depth, thickness and magnitude coincide with large eddy amplitudes. This new knowledge is expected to help to advance our understanding of the variability in marine primary production in the South China Sea.

# 1. Introduction

Subsurface chlorophyll maximum (SCM) layers show up as pronounced peaks in vertical profiles of chlorophyll (Chl) and are widespread features of stratified open oceans (Cullen 2015, Yasunaka et al. 2022). They play a crucial role in the global carbon cycle, especially in supporting secondary carbon production and exporting carbon to the deep ocean (Silsbe and Malkin 2016, Takahashi and Hori 1984). Previous studies have suggested that SCM layer could contribute substantially to the vertically integrated biomass (~55%, Takahashi and Hori 1984) and to the depth-integrated primary production (16~42%, Barbieux et al. 2022) in the oligotrophic stratified open ocean. Further insight into the mechanisms underlying SCM layer variability could advance our understanding of global carbon cycling.

Mesoscale eddies have profound effects on the lateral and vertical distributions of the physical and biogeochemical properties of seawater throughout the global ocean (Amos et al. 2019, Chaigneau et al. 2011, Gaube et al. 2014, McGillicuddy 2016, Zhan et al. 2019). The spatial–temporal variability and mechanisms of eddy-induced Chl in the surface ocean have been extensively examined through the analyses of ocean color satellite images (Frenger et al. 2018, Gaube and McGillicuddy 2017, Gaube et al. 2014, Siegel et al. 1999). The variability of phytoplankton in the mesoscale eddy field is modulated by eddy transport (such as stirring and trapping), eddy pumping and eddy-Ekman pumping because of vertical nutrient fluxes (McGillicuddy 2016, Siegel et al. 2011). However, ocean color satellite images are unable to capture the SCM layer.

Therefore, SCM data with sufficiently high temporal and spatial resolutions are limited and the impact of mesoscale eddies on subsurface Chl is poorly understood. Targeted surveys in specific areas over a short period have shown that the SCM layer becomes shallower and increases in magnitude in cyclonic eddies; it increases in depth and decreases in magnitude in anticyclonic eddies (Barone et al. 2022, Huang and Xu 2018, Wang et al. 2018, He et al. 2019, Xu et al. 2022). Mesoscale eddies bringing episodic pulses of deep nutrients into the euphotic zone play a major role in sustaining positive net community production in the North Pacific subtropical gyre (Johnson et al. 2010). The size composition of phytoplankton in the subsurface layer is markedly different in cyclonic eddies compared to background (Benitez-Nelson et al. 2007, Hernández-Hernández et al. 2020). Biogeochemical Argo (BGC-Argo) floats are considered to be one of the most promising approaches for assessing the influence of eddies on subsurface biomass (Su et al. 2021, Cornec et al. 2021). Cornec et al. (2021) suggested that at the global scale, cyclonic eddies increase SCM magnitude and biomass, while SCM magnitudes in anticyclonic eddies are small. However, the availability of field measurements is limited in terms of spatial and temporal coverage and parameter types, which hinders the quantitative assessment of changes in the SCM layers associated with ephemeral mesoscale processes such as mesoscale eddies.

Physical–biogeochemical models are useful tools for the analysis of the variability of subsurface Chl under the influence of physical processes such as upwelling, eddies, fronts and sub-mesoscale currents (Gan et al. 2010, Guo et al. 2017, Lévy et al. 2018,

Xiu and Chai 2011). The fully coupled physical–ecosystem model developed by the Darwin project of the Massachusetts Institute of Technology (https://darwinproject.mit.edu) has been successful in modelling the key phytoplankton size classes and seasonal/intra-seasonal variation of surface Chl (Qin et al. 2022) and has already been used by several research groups to study phytoplankton community structure (Benoiston et al. 2017, Kuhn et al. 2019, Mangolte et al. 2022). This well-tested and eddy-permitting model is useful for studying the impact of mesoscale eddies on SCM characteristics and phytoplankton community.

The South China Sea (SCS) is the largest semi-enclosed marginal sea in the western Pacific Ocean with active mesoscale eddies (Chen et al. 2011, Hu et al. 2011, Wang et al. 2008, Xiu et al. 2010). It serves as an ideal test bed for studying the spatial structure and lifecycle of mesoscale eddies (Zhang et al. 2016b). Eddy-induced upwelling and associated nutrient transport have prominent effects on phytoplankton growth and productivity in the open SCS (Huang et al. 2010, Ning et al. 2004, Wang et al. 2016, Wang et al. 2018, Zhang et al. 2016a), which is categorized as oligotrophic waters (Wong et al. 2007). Chen et al. (2007) suggested that the concentrations of biogeochemical parameters in the Luzon Strait during an unproductive season are even higher than in winter because of high eddy activity. The SCM is a recurrent and widespread phenomenon (Gong et al. 2014) and makes considerable contributions to phytoplankton biomass and production in the open SCS (Ning et al. 2004). In situ measurements show that anticyclonic eddies increase SCM depth and reduce SCM

magnitude (Xing et al. 2019, Xu et al. 2022). Additionally, the water-column integrated biomass was enhanced at the anticyclonic eddy edges and the fraction of diatom was also increased (Wang et al. 2018). Using a coupled three-dimensional physical–biogeochemical model, Xiu and Chai (2011) found considerable enhancement of depth-integrated phytoplankton biomass in cyclonic eddies in the SCS basin. Nutrient supply and weakening of the light intensity below the surface layer synergistically influenced the size structure of phytoplankton in the different eddy polarity at different depths (Liang et al. 2018). The impact of eddies on the phytoplankton in the subsurface layer and their main driving mechanisms in the SCS are still poorly understood partly because of the limited availability of in situ observations and the relatively simplicity of existing physical biogeochemical models. Therefore, in this study, we analyzed MITgcm Darwin model with a well physical framework and sophisticated biogeochemical model output to examine the impact of eddies on SCM characteristics (including SCM depth, thickness and magnitude) and phytoplankton community in the SCS.

## 2. Material and Methods

### 2.1 Model description and validation

We used model outputs from a coupled physical–ecosystem model based on the MITgcm (https://doi.org/10.6075/J0BR8QJ1; Jahn et al., 2019) and analyzed physical and biogeochemical parameters including 3-day means of sea surface height (SSH),

temperature, salinity and various phytoplankton biomass and environmental parameters from December 1993 to December 2015. The model uses the configuration of the ECCO2 CS510 physical simulation; it has a mean horizontal grid spacing of 18 km and 50 levels in the vertical direction, which ensures realistic representation of eddy formation (Menemenlis et al. 2008). The ecosystem and biogeochemical components of this model are based on Dutkiewicz et al. (2015), which incorporate both functional and size diversity of plankton. The model features parameterizations based on Ward et al. (2012) and resolves a total of 51 plankton types (35 types of phytoplankton and 16 types of zooplankton). Cycling of carbon, phosphorus, nitrogen, silica, iron, and oxygen are included in the model. In this study, we included six functional groups in our phytoplankton community analyses; they are prokaryotes, picoeukaryotes, coccolithophores, diazotrophs, diatoms and mixotrophic dinoflagellates.

The model successfully reproduces the regional and seasonal patterns of total Chl and key phytoplankton community structures in the surface ocean (Kuhn et al. 2019). Vertical distributions of temperature, salinity and Chl concentration from the model outputs agree well with the measured profiles by the BGC-Argo in the northern South China Sea between July 2014 and December 2015 (Figure 1). Zhang et al.（2016）and Xing et al. (2019) analyzed the same float data and identified a SCM and a deep mixed layer. The modeled SCM depth is generally consistent with BGC-Argo data. The model replicates the observed winter bloom, while the intensity of bloom is weaker than the measured. Model performance is further evaluated using scatter plot and liner

regression analysis (Figure 2). Good fit is found for temperature and Chl concentration with the slopes of regression lines nearly 1. The $R^2$ of the linear regressions are very high (0.9) for temperature, and are relatively lower for salinity (0.68) and Chl concentration (0.42). Because the BGC-Argo observations were discrete in both temporal and spatial, the results of vertical profiles comparison for this long time-series were valuable although there were some discrepancies. Furthermore, the undulations in the subsurface spatial variability of Chl and other environmental parameters were apparently well captured by the model and comparable with the observations albeit the magnitude was underestimated in the model.

**2.2 SCM parameters**

To characterize the SCM layer qualitatively and quantitatively, we calculated the values of three key parameters: the thickness, depth and magnitude of the SCM. The SCM depth is defined as the depth at which Chl concentration is maximum; SCM magnitude is defined as the Chl concentration at the SCM depth. In previous studies, the thickness of this layer was either ignored or determined by ad hoc choices (Beckmann and Hense 2007, Letelier et al. 2004, Pérez et al. 2006). We fitted the Chl model output to an exponential power law function (Equation 1) and used it to calculate SCM thickness. It is important to note that Chl profile with the SCM depth shallower than mixed layer depth was excluded in this study. Those Chl profiles mainly presented in the northern SCS in winter, accounting for less than 1% of the total Chl profiles.

We interpolated the Chl output from a coarse vertical grid (resolution of

approximately 10 m) on to a finer grid (resolution of approximately 1 m). Then, the profile at each grid point was fitted by:

$$Chl_{mod}(z) = a + b\left(\frac{p}{2\sigma\Gamma(\frac{1}{p})}e^{-|\frac{z-\mu}{\sigma}|^p}\right),\ldots\ldots\ldots\ldots\ldots\ldots\ldots\ldots\ldots\ldots\ldots\ldots\ldots\ldots\ldots(1)$$

where *Chl~mod~* represents fitted Chl; *a* is the background Chl; z is depth; *b* is a scale factor to adjust SCM magnitude to take into account background Chl; $\left(\frac{p}{2\sigma\Gamma(\frac{1}{p})}e^{-|\frac{z-\mu}{\sigma}|^p}\right)$ is the exponential power distribution that determines the structure of the Chl profile; p is the factor controlling the tail region and the shape of the distribution; Γ represents the gamma function. Previous studies have demonstrated that the exponential power law (Equation 1) is an appropriate approximation of the Chl profile (Leach et al. 2018, Xu et al. 2022). When SCM depth is less than σ, the thickness of the SCM layer is defined as the sum of μ and σ; otherwise, SCM thickness is 2σ.

Most of the Chl profiles had p values below 2 (~90%), and only approximately ~5% had a p value close to 2. Our results indicated that exponential power distribution function could effectively describe Chl profiles with a flat Chl peak or a sharp Chl peak, which is more superior to the gaussian-type distribution function.

**2.3 Eddy detection and tracking**

Using the 3-day mean gridded SSH data, mesoscale eddies were detected and tracked by applying the eddy tracking algorithm developed by Faghmous et al. (2015), which defines eddies as the outermost closed-contour SSH containing a single extreme. Several eddy parameters were computed, including the position, the amplitude and the radius R of the core. We only retained eddies with minimum amplitudes that exceeded

11

1 cm and lifetimes of over 30 days to exclude small-scale noisy structures. In total, we identified 1548 eddy trajectories in the SCS between 1994 and 2015; the number of anticyclonic eddies (673) was close to that of cyclonic eddies (875).

**2.4 Composite analysis**

We estimated horizontal composite anomalies of SCM characteristics and other environmental factor induced by mesoscale eddies in the South China Sea. To investigate SCM characteristics variability induced by mesoscale eddies, SCM characteristics anomalies were calculated as the difference between the values from 1994–2015 and climatological monthly means for each grid point. Other environmental factors anomalies in the SCM layer were also calculated using the same method. It is worth noting that the relative anomalies (hereinafter referred to as anomalies) are calculated by dividing anomalies by the climatological monthly means.

Further, we matched eddies and Chl profiles with SCM layer by following steps. For each available Chl profile with SCM layer, we identified all eddies that were observed on the same date. We then calculated the distance from each eddy center to the Chl profiles. A profile was matched to an eddy if it was < 1.5R from the eddy center. If a profile could be matched with more than one eddy, the closest eddy was chosen as the matching eddy.

**2.5 Definition and calculation of other supplementary parameters**

The mixed-layer depth is calculated as the depth where the density value is 0.03 kg m$^{-3}$ greater than the value at 10 m (Montégut et al. 2004). Euphotic depth ($Z_{eu}$) is

the depth at which photosynthetic available radiation is 1% of its surface value. Then

the integrated Chl concentrations between the surface and the euphotic depth ($\Sigma Chl_{Zeu}$)

is also calculated. Nitracline depth is the depth at which the first derivative of the nitrate

concentration along the vertical is maximum. We identify first derivatives that

were >75 % of the first derivative at the nitracline; their mean was the nitracline slope.

## 3. Results

The number of eddy centroids that passed through each 1°×1° grid square over

the 22-year period of December 1993 to December 2015 is shown in Figure 3a. There

were large numbers of mesoscale eddies over the northern SCS, and the eddy-rich

regions coincided with regions of large standard deviations of SSH (Figure 3b); this

indicates the importance of eddies in SSH variability in the SCS. The characteristics of

the eddies in the SCS are summarized in Table 1. The amplitudes of mesoscale eddies

ranged from about 1 cm to over 40.8 cm, with mean values of 6.9 cm for cyclonic and

7 cm for anticyclonic eddies (Figure 3c and Table 1). Eddy radii ranged from about 30

km to over 333 km, with median values of 92.1 km for cyclonic and 104.9 km for

anticyclonic eddies (Figure 3d and Table 1). These values are comparable to those

reported by previous studies (Chen et al. 2011, Xiu et al. 2010, He et al. 2019) and

indicate the reliability of the model.

Hydrographic sections of nutrients and Chl anomaly across the anticyclonic and

cyclonic eddies are presented in Figure 4. The hydrological structures of the composited

eddies were consistent with expectations based on eddy polarity: anticyclonic eddies

are characterized by a depressed thermoclines with positive temperature anomalies (Figure 4a), while cyclones demonstrated shallower thermoclines with negative temperature anomalies (Figure 4b). Cyclonic eddy enhanced the supply of inorganic nutrient to the upper layer by lifting the thermocline and increased the concentrations of Chl (Figure 4c, d), while downward displacement of thermocline in anticyclonic eddies moved the deep reservoir of inorganic nutrients further away from the euphotic zone and decreased the concentrations of Chl (Figure 4a, b). In isopycnal coordinates, the concentrations of Chl in the upper layer of the anticyclonic eddies decreased, but the concentrations of nutrients increased (Figure S1a, c), and vice versa in the cyclonic eddies (Figure S1b, d).

Figure 5 shows the composite spatial patterns of SCM depth, magnitude and thickness in mesoscale eddies in the SCS normalized by eddy radius. In most cases, anomalies were approximately symmetrically distributed around a maximum at the center and decayed radially toward the eddy boundary (Figure 5a–e), although the maximal thickness anomaly caused by anticyclonic eddies drifted away from the center (Figure 5f). The eddy-induced SCM thickness decreased considerably in cyclonic eddies and increased slightly in anticyclonic eddies (Figure 5c, f); this result has not been reported by previous studies. Near the center of cyclonic eddies, SCM depth, magnitude and thickness anomalies were on the order of $-11\% \pm 15\%$, $12\% \pm 21\%$ and $-11\% \pm 24\%$, respectively. Cyclonic eddies reduce SCM depth; as a result, depth anomalies were negative near eddy centers (Figure 5a). Cyclonic eddies increased

SCM magnitude and reduced SCM thickness (Figure 5b, c). Anticyclonic eddies were near mirror images of cyclonic eddies (Figure 5d–f). Near the center of anticyclonic eddies, SCM depth, magnitude and thickness anomalies were on the order of $11\% \pm 19\%$, $-10\% \pm 16\%$ and $6\% \pm 28\%$, respectively. In addition, the impact of the eddy on the SCM characteristics had a weak seasonal variability (Figure S2).

In anticyclonic eddies, the SCM depth increased and water density decreased, while the SCM depth decreased and density increased in cyclonic eddies (Figure 6). Cyclonic eddies bring isopycnal surfaces closer to the surface (Figure 4); as these isopycnal surfaces move downward, unused nutrients and organic matter that have accumulated in the surface water with lower density are also transported downward (Benitez-Nelson et al. 2007). The density anomaly could also be positive in the boundaries of anticyclonic eddies, which may be related to the sub-mesoscale dynamic processes in the periphery.

We investigated the relationship between eddy-induced anomalies and eddy amplitude, which has received little attention in previous studies. Figure 7 shows that eddy-induced SCM depth and magnitude anomalies increased with eddy amplitude in both cyclonic and anticyclonic eddies. Depth anomaly typically grew by about 1% for each 1 cm increase in eddy amplitude ($R^2$=0.730 for anticyclonic eddy, $R^2$=0.842 for cyclonic eddy) (Figure 7a). For both cyclonic and anticyclonic eddies, SCM magnitude increased by about 2% for each 1 cm increase of eddy amplitude ($R^2$=0.944 for anticyclonic eddy, $R^2$=0.900 for cyclonic eddy) (Figure 7b). In contrast, the relationship

between the thickness anomaly and eddy amplitude in cyclonic eddies was different from that in anticyclonic eddies. For cyclonic eddies, thickness decreased linearly with increasing amplitude ($R^2$=0.939); for anticyclonic eddies, thickness only increased slightly with amplitude ($R^2$=0.066) (Figure 7c). In addition, the temporal evolution of SCM layer over mesoscale eddy lifecycles was also investigated. Those eddies with lifetimes that first intensify and then weaken monotonically are selected (Figure S3) and then divided into five stages. The impact of eddy on SCM layer has slightly difference with different eddy life stages (Figure S4). Near the center of cyclonic (anticyclonic) eddies, the maximum anomalies of SCM depth, magnitude and thickness presented in maturity stage and were on the order of $-14\%$ (12%) , 18% ($-12\%$) and $-16\%$ (6%), respectively.

The eddy-induced Chl anomalies in the surface layer ($Chl_{surf}$) and those that have been integrated vertically across the euphotic layer ($\Sigma Chl_{Zeu}$) are shown in Figures 8a and 9. Cyclonic (anticyclonic) eddies enhanced (reduced) $Chl_{surf}$ and $\Sigma Chl_{Zeu}$. This implies that the phytoplankton biomass could be enhanced within cyclonic eddies, while anticyclonic eddies tended to suppress phytoplankton biomass. In cyclonic eddies, the maxima of $Chl_{surf}$ and $\Sigma Chl_{Zeu}$ did not coincide with where they appeared in the composite map (Figure 9a, c).

The phytoplankton community structure perturbations associated with mesoscale eddies in the surface layer differed from those in the subsurface layer (Figure 8b, c). In the surface layer, mesoscale eddies induced an anomaly in the fraction of pico-

prokaryotes; anticyclonic eddies induced an increase in the pico-prokaryote fraction while cyclonic eddies induced a decrease. However, in the subsurface layer, cyclonic eddies led to a shift in phytoplankton assemblage composition. Cyclonic eddies resulted in an increased fraction of diatoms (0.04±0.06) while anticyclonic eddies resulted in an increase fraction of coccolithophores (0.03±0.05). Fraction anomalies of the other four plankton types were relatively small; they were all negative in cyclonic eddies and all positive in anticyclonic eddies.

Figure 10a shows that the depth (slope) of the nitracline was reduced (increased) in cyclonic eddies. As a result, nutrient supply to the euphotic zone was enhanced and the concentrations of nutrients (dissolved inorganic nitrogen DIN, which is the sum of nitrate, nitrite and ammonia) and photosynthetically active radiation (PAR) in SCM layers increased in cyclonic eddies (Figure 10b). In response to the environmental perturbations caused by cyclonic eddies, SCM depth decreased and magnitude increased (Figure 7a, b). In contrast, the nitraclines associated with anticyclonic eddies were deeper and flatter (Figure 10a), and resulted in negative DIN and PAR anomalies in SCM layers (Figure 10b). Because of a shortage of light and nutrients, phytoplankton in SCM layers in anticyclonic eddies grew slowly and SCM depth increased and magnitude decreased (Figure 7d, e). There was a linear relationship between the eddy-induced anomalies in environmental factors and eddy amplitude (color shading in Figure 10).

The relationships between nitracline depth (slope) and SCM characteristics were

furtherly investigated in our study. We found that the nitracline depth is a dominant factor to adjust the variability of SCM depth, with a robust positive correlation ($R^2$=0.456) (Figure 11a). The magnitude of SCM was affected by the nitracline depth but also nitracline slope, and the shallow and steep nitraclines were usually accompanied by large SCM magnitude (Figure 11c and 11d). Although there was weak relationship between the SCM thickness and nitracline depth (slope), we also found that the thicker SCM layers generally appear within the deep and flatter nitracline (Figure 11e and 11f). Therefore, when investigating the causes of SCM characteristic changes, it is necessary to analyze the changes of nitracline depth and slope simultaneously.

## 4. Discussions

Based on 22 years of an eddy-permitting biological–physical coupled model output data, an opportunity is provided to assess the impact of eddies on SCM characteristics in the SCS. By composite analysis, we find robust differences between cyclones and anticyclones in the depth, thickness and magnitude of SCM layer. Furthermore,  the effects of eddies on phytoplankton communities are related to eddy polarity and depth.

In nutrient replete regions, phytoplankton assemblage structures are usually dominated by large-celled species (Pingree et al. 1976). In nutrient deplete environments, small-celled species tend to dominate (Irwin et al. 2006, Munk and Riley 1952), possibly because of their ability to take up nutrients at low concentrations (Sigman and Hain 2012). Our results show that the fraction of pico-prokaryotes

increases (decreases) in the surface layer in anticyclonic (cyclonic) eddies (Figure 8b). In the subsurface layer, the fraction of diatoms (coccolithophores) increases (decreases) in cyclonic (anticyclonic) eddies (Figure 8c); this is consistent with previous studies that indicated that coccolithophores rapidly rise to dominate over diatoms as the nitracline deepens (Cermeno et al. 2008). Nutrient limitation can impact the competition between diatoms and coccolithophores and have profound implications on the efficiency of biological pumps (Cermeno et al. 2008). In addition, the distribution of phytoplankton community may also be associated with eddy retention time. Longer retention time inside cyclonic eddies are likely to favor slowly sinking plankton (such as diatoms), while shorter retention time inside anticyclonic eddies are likely to favor upward motile plankton (Condie and Condie 2016).

In this study, we identified the impact of mesoscale eddies on SCM depth, magnitude and thickness, and phytoplankton community structure in the SCS. However, the regional and seasonal variability of the influence of eddies on SCM characteristics remains unclear. There is considerable regional variability in eddy characteristics (Chen et al. 2011) and a strong seasonal signal in the eddy-induced surface Chl variability in the SCS (He et al. 2016). In winter, the SCM layer in the northern SCS disappeared due to deep mixing induced by wind and buoyancy forcing. In order to focus as much as possible on the impact of eddies on the SCM layer, Chl profiles with SCM depths shallower than the mixed layer depth were excluded from this study. Nonetheless, failure to consider seasonal variation might lead to biases in the estimation of the impact

of eddies on SCM characteristics. In addition, the intensity and decay period of an eddy is complex because eddies can increase and decrease intensity multiple times during its lifetime due to eddy-to-eddy interactions and eddy-flow interactions. Differences in the origin and age of anticyclonic eddies could also result in different effects on phytoplankton community in the SCS (Huang et al. 2010). Further studies on the spatial and seasonal variability of SCM characteristics associated with mesoscale eddies are needed.

It is generally accepted that the formation of phytoplankton is most likely affected by submesoscale processes occurring along the periphery of eddies, where the vertical velocities are significant (Capet et al. 2008, Peterson et al. 2011). The asymmetric structure in composite map of SCM thickness may related to the submesoscale processes along the periphery of anticyclonic eddies. Meanwhile, the asymmetric structures induced by submesoscale processes are also found in both observation (Tang et al. 2019) and simulation results (Brannigan et al. 2016). Given the phytoplankton are restricted to the euphotic zone where light is available for photosynthesis, the SCM thickness cannot continue to increase in anticyclonic eddies. As a result, the SCM thickness anomaly may show weakly positive linear tend in the anticyclonic eddies.

The most common manifestations of mesoscale eddies regulating the rates of biological processes are related to vertical movements which can affect the availability of both light and nutrients to phytoplankton and thereby alter the growth of phytoplankton (Cullen 2015, Li et al. 2021). Mesoscale eddies affect phytoplankton

distribution and hence Chl concentrations via different mechanisms, such as nutrient pumping associated with eddy intensification (Falkowski et al. 1991, McGillicuddy 2016), diapycnal nutrient fluxes as a result of the steeper vertical gradients in inorganic nutrients caused by eddies (Barone et al. 2022) and the redistribution of nutrients in the euphotic zone due to eddy-induced vertical oscillations of the pycnocline (Falkowski et al. 1991). Previous studies emphasize the optimization of opposing gradients in light and nutrient fluxes in SCM layers (Cullen 2015, Letelier et al. 2004). Recent studies suggest that interactions and feedbacks between iron and light availability might also play important roles in controlling SCM dynamics (Hawco et al. 2021, Hogle et al. 2018). In this study, we analyzed the variability of light availability and nutrient fluxes in SCM layers. Further studies are needed to examine iron and other critical nutrients induced by eddies and SCM dynamics in the SCS.

## 5. Conclusion

The SCM layers can account for a notable fraction of the total biomass and primary production in the water column. In this study, we examined SCM depth, magnitude and thickness in response to mesoscale eddies in the SCS using a coupled ocean–ecosystem model. Figure 12 summarizes the relationship between mesoscale eddies and SCM characteristics. Anticyclonic eddies generally increase SCM depth and thickness and reduce SCM magnitude, while cyclonic eddies reduce SCM depth and thickness and increase SCM magnitude. Composite analyses of large numbers of eddies indicate that

anomalies are the largest at the center of the eddy and decrease toward the eddy boundary. Phytoplankton community structures in SCM layers are also clearly affected by eddies. In cyclonic eddies, the fraction of diatoms increases and coccolithophores are abundant in anticyclonic eddies. The effect of eddies on SCM properties increases with eddy amplitude.

## Acknowledgments

## Data Availability Statement

Model data used in this study are publicly available at: https://doi.org/10.6075/J0BR8QJ1 (Jahn et al. 2016). Figures were made with Matlab version 9.12.0.1884302 (R2022a), available under the Matlab license at https://www.mathworks.com/products/matlab.html (Matlab, 2022).

# References

Amos CM, Castelao RM, Medeiros PM. 2019. Offshore transport of particulate organic carbon in the California Current System by mesoscale eddies. Nat Commun 10:4940.

Barbieux, M., Uitz, J., Mignot, A., Roesler, C., Claustre, H., Gentili, B., Taillandier, V., D'Ortenzio, F., Loisel, H., Poteau, A., Leymarie, E., Penkerc'h, C., Schmechtig, C., & Bricaud, A. 2022. Biological production in two contrasted regions of the Mediterranean Sea during the oligotrophic period: an estimate based on the diel cycle of optical properties measured by BioGeoChemical-Argo profiling floats. Biogeosciences, 19, 1165-1194

Barone B, Church MJ, Dugenne M, Hawco NJ, Jahn O, White AE, John SG, Follows MJ, DeLong EF, Karl DM. 2022. Biogeochemical Dynamics in Adjacent Mesoscale Eddies of Opposite Polarity. Global Biogeochemical Cycles 36.

Beckmann A, Hense I. 2007. Beneath the surface: Characteristics of oceanic ecosystems under weak mixing conditions – A theoretical investigation. Progress in Oceanography 75:771-796.

Benitez-Nelson CR, et al. 2007. Mesoscale Eddies Drive Increased Silica Export in the Subtropical Pacific Ocean. 316:1017-1021.

Benoiston AS, Ibarbalz FM, Bittner L, Guidi L, Jahn O, Dutkiewicz S, Bowler C. 2017. The evolution of diatoms and their biogeochemical functions. Philos Trans R Soc Lond B Biol Sci 372.

Brannigan, L. 2016, Intense submesoscale upwelling in anticyclonic eddies, Geophys. Res. Lett., 43, 3360–3369, doi:10.1002/2016GL067926.

Capet, X, McWilliams, J. C, Molemaker, M. J, & Shchepetkin, A. F. 2008. Mesoscale to submesoscale transition in the California Current System. Part I: Flow structure, eddy flux, and observational tests. Journal of Physical Oceanography, 38(1), 29–43. https://doi.org/10.1175/2007jpo3671.1

Cermeno P, Dutkiewicz S, Harris RP, Follows M, Schofield O, Falkowski PG. 2008. The role of nutricline depth in regulating the ocean carbon cycle. Proc Natl Acad Sci U S A 105:20344-20349.

Chaigneau A, Le Texier M, Eldin G, Grados C, Pizarro O. 2011. Vertical structure of mesoscale eddies in the eastern South Pacific Ocean: A composite analysis from altimetry and Argo profiling floats. Journal of Geophysical Research: Oceans 116.

Chen G, Hou Y, Chu X. 2011. Mesoscale eddies in the South China Sea: Mean properties, spatiotemporal variability, and impact on thermohaline structure. Journal of Geophysical Research 116.

Condie S, Condie R. 2016. Retention of plankton within ocean eddies. Global Ecology and Biogeography 25:1264-1277.

Cornec M, Laxenaire R, Speich S, Claustre H. 2021. Impact of Mesoscale Eddies on Deep Chlorophyll Maxima. Geophys Res Lett 48:e2021GL093470.

Cullen JJ. 2015. Subsurface chlorophyll maximum layers: enduring enigma or mystery solved? Ann Rev Mar Sci 7:207-239.

Dutkiewicz, S., A. E. Hickman, O. Jahn, W. W. Gregg, C. B. Mouw, and M. J. Follows (2015), Capturing optically important constituents and properties in a marine biogeochemical and ecosystem model, Biogeosciences, 12(14), 4447-4481, doi:10.5194/bg-12-4447-2015.

Faghmous JH, Frenger I, Yao Y, Warmka R, Lindell A, Kumar V. 2015. A daily global mesoscale ocean eddy dataset from satellite altimetry. Sci Data 2:150028.

Mesoscale eddy modulation of subsurface chlorophyll maximum layers in the South China Sea

Falkowski PG, Ziemann D, Kolber Z, Bienfang PK. 1991. Role of eddy pumping in enhancing primary production in the ocean. Nature 352:55-58.

Frenger I, Münnich M, Gruber N. 2018. Imprint of Southern Ocean mesoscale eddies on chlorophyll. Biogeosciences 15:4781-4798.

Gan J, Lu Z, Dai M, Cheung AYY, Liu H, Harrison P. 2010. Biological response to intensified upwelling and to a river plume in the northeastern South China Sea: A modeling study. Journal of Geophysical Research 115.

Gaube P, McGillicuddy DJ. 2017. The influence of Gulf Stream eddies and meanders on near-surface chlorophyll. Deep Sea Research Part I: Oceanographic Research Papers 122:1-16.

Gaube P, McGillicuddy Jr DJ, Chelton DB, Behrenfeld MJ, Strutton PG. 2014. Regional variations in the influence of mesoscale eddies on near‐surface chlorophyll. Journal of Geophysical Research: Oceans 119:8195-8220.

Gong X, Shi J, Gao H. 2014. Modeling seasonal variations of subsurface chlorophyll maximum in South China Sea. Journal of Ocean University of China 13:561-571.

Guo L, Xiu P, Chai F, Xue H, Wang D, Sun J. 2017. Enhanced chlorophyll concentrations induced by Kuroshio intrusion fronts in the northern South China Sea. Geophysical Research Letters 44.

Hawco NJ, et al. 2021. Iron Depletion in the Deep Chlorophyll Maximum: Mesoscale Eddies as Natural Iron Fertilization Experiments. Global Biogeochemical Cycles 35.

He Q, Zhan H, Cai S, Li Z. 2016. Eddy effects on surface chlorophyll in the northern South China Sea: Mechanism investigation and temporal variability analysis. Deep Sea Research Part I: Oceanographic Research Papers 112:25-36.

He, Q., Zhan, H., Xu, J., Cai, S., Zhan, W., Zhou, L., & Zha, G. (2019). Eddy-Induced Chlorophyll Anomalies in the Western South China Sea. Journal of Geophysical Research: Oceans, 124, 9487-9506

Hernández-Hernández N, Arístegui J, Montero MF, Velasco-Senovilla E, Baltar F, Marrero-Díaz Á, Martínez-Marrero A, Rodríguez-Santana Á. 2020. Drivers of Plankton Distribution Across Mesoscale Eddies at Submesoscale Range. Frontiers in Marine Science 7.

Hogle SL, et al. 2018. Pervasive iron limitation at subsurface chlorophyll maxima of the California Current. Proc Natl Acad Sci U S A 115:13300-13305.

Hu J, Gan J, Sun Z, Zhu J, Dai M. 2011. Observed three-dimensional structure of a cold eddy in the southwestern South China Sea. Journal of Geophysical Research 116.

Huang B, Hu J, Xu H, Cao Z, Wang D. 2010. Phytoplankton community at warm eddies in the northern South China Sea in winter 2003/2004. Deep Sea Research Part II: Topical Studies in Oceanography 57:1792-1798.

Huang J, Xu F. 2018. Observational Evidence of Subsurface Chlorophyll Response to Mesoscale Eddies in the North Pacific. Geophysical Research Letters 45:8462-8470.

Irwin AJ, Finkel ZV, Schofield OM, Falkowski PG. 2006. Scaling-up from nutrient physiology to the size-structure of phytoplankton communities. Journal of Plankton Research 28:459-471.

Johnson KS, Riser SC, Karl DM. 2010. Nitrate supply from deep to near-surface waters of the North Pacific subtropical gyre. Nature 465:1062-1065.

Jahn, Oliver; Hill, Christopher; Dutkiewicz, Stephanie; Follows, Michael (2019). MITgcm 3-daily global sea surface temperature, ocean currents, nitrate and phytoplankton biomass from 1992 to

Mesoscale eddy modulation of subsurface chlorophyll maximum layers in the South China Sea

2016 [Dataset]. UC San Diego Library Digital Collections. https://doi.org/10.6075/J0BR8QJ1

Kuhn, A. M., S. Dutkiewicz, O. Jahn, S. Clayton, T. A. Rynearson, M. R. Mazloff, and A. D. Barton. 2019, Temporal and Spatial Scales of Correlation in Marine Phytoplankton Communities, Journal of Geophysical Research: Oceans, 124(12), 9417-9438, doi:10.1029/2019jc015331.

Leach TH, et al. 2018. Patterns and drivers of deep chlorophyll maxima structure in 100 lakes: The relative importance of light and thermal stratification. Limnology and Oceanography 63:628-646.

Letelier RM, Karl DM, Abbott MR, Bidigare RR. 2004. Light driven seasonal patterns of chlorophyll and nitrate in the lower euphotic zone of the North Pacific Subtropical Gyre. Limnology and Oceanography 49:508-519.

Lévy M, Franks PJS, Smith KS. 2018. The role of submesoscale currents in structuring marine ecosystems. Nature Communications 9.

Li R, Xu J, Cen X, Zhong W, Liao J, Shi Z, Zhou S. 2021. Nitrate fluxes induced by turbulent mixing in dipole eddies in an oligotrophic ocean. Limnology and Oceanography 66:2842-2854.

Liang W, Tang D, Luo X. 2018. Phytoplankton size structure in the western South China Sea under the influence of a 'jet-eddy system'. Journal of Marine Systems 187:82-95.

Mangolte I, Lévy M, Dutkiewicz S, Clayton S, Jahn O. 2022. Plankton community response to fronts: winners and losers. Journal of Plankton Research.

Matlab. (2022). Matlab: February 16, 2022 release (version 9.12.0.1884302) [Software]. Matlab. Retrieved from https://www.mathworks.com/ products/matlab.html

McGillicuddy DJ, Jr. 2016. Mechanisms of Physical-Biological-Biogeochemical Interaction at the Oceanic Mesoscale. Ann Rev Mar Sci 8:125-159.

Menemenlis D, Campin J-M, Heimbach P, Hill C, Lee T, Nguyen A, Schodlok M, Zhang H. 2008. ECCO2: High resolution global ocean and sea ice data synthesis. AGU Fall Meeting Abstracts.

Montégut, C. d. B., G. Madec, A. S. Fischer, A. Lazar, and D. Iudicone. 2004, Mixed layer depth over the global ocean: An examination of profile data and a profile-based climatology, Journal of Geophysical Research, 109(C12), doi:10.1029/2004jc002378.

Munk, Walter H., and Gordon A. Riley. 1952. Absorption of nutrients by aquatic plants. Journal of Marine Research 11, (2).

Ning X, Chai F, Xue H, Cai Y, Liu C, Shi J. 2004. Physical-biological oceanographic coupling influencing phytoplankton and primary production in the South China Sea. Journal of Geophysical Research 109.

Pérez V, Fernández E, Marañón E, Morán XAG, Zubkov MV. 2006. Vertical distribution of phytoplankton biomass, production and growth in the Atlantic subtropical gyres. Deep Sea Research Part I: Oceanographic Research Papers 53:1616-1634.

Peterson, T. D, Crawford, D. W, & Harrison, P. J. 2011. Mixing and biological production at eddy margins in the eastern Gulf of Alaska. Dee Sea Research Part-I Oceanographic Research Papers, 58(4), 377–389. https://doi.org/10.1016/j.dsr.2011.01.010

Pingree R, Holligan P, Mardell G, Head R. 1976. The influence of physical stability on spring, summer and autumn phytoplankton blooms in the Celtic Sea. Journal of the Marine Biological Association of the United Kingdom 56:845-873.

Qin J, Meng Z, Xu W, Li B, Cheng X, Murtugudde R. 2022. Modulation of the intraseasonal chlorophyll‐a concentration in the tropical Indian Ocean by the Central Indian Ocean Mode.

Mesoscale eddy modulation of subsurface chlorophyll maximum layers in the South China Sea

Geophysical Research Letters.

Seki MP, Polovina JJ, Brainard RE, Bidigare RR, Leonard CL, Foley DG. 2001. Biological enhancement at cyclonic eddies tracked with GOES Thermal Imagery in Hawaiian waters. Geophysical Research Letters 28:1583-1586.

Siegel DA, McGillicuddy DJ, Fields EA. 1999. Mesoscale eddies, satellite altimetry, and new production in the Sargasso Sea. Journal of Geophysical Research: Oceans 104:13359-13379.

Siegel DA, Peterson P, McGillicuddy DJ, Maritorena S, Nelson NB. 2011. Bio-optical footprints created by mesoscale eddies in the Sargasso Sea. Geophysical Research Letters 38.

Sigman DM, Hain MPJNEK. 2012. The biological productivity of the ocean. Nature Education 3:1-16.

Silsbe GM, Malkin SY. 2016. Where light and nutrients collide: The global distribution and activity of subsurface chlorophyll maximum layers. Pages 141-152. Aquatic microbial ecology and biogeochemistry: A dual perspective, Springer.

Su J, Strutton PG, Schallenberg C. 2021. The subsurface biological structure of Southern Ocean eddies revealed by BGC-Argo floats. Journal of Marine Systems 220.

Takahashi M, Hori T. 1984. Abundance of picophytoplankton in the subsurface chlorophyll maximum layer in subtropical and tropical waters. Marine Biology 79:177-186.

Tang, Q, Gulick, S. P. S, Sun, J, Sun, L, & Jing, Z. 2020. Submesoscale features and turbulent mixing of an oblique anticyclonic eddy in the Gulf of Alaska investigated by marine seismic survey data. Journal of Geophysical Research: Oceans, 125, e2019JC015393. https://doi.org/10.1029/2019JC015393

Wang G, Chen D, Su J. 2008. Winter Eddy Genesis in the Eastern South China Sea due to Orographic Wind Jets. Journal of Physical Oceanography 38:726-732.

Wang L, Huang B, Chiang KP, Liu X, Chen B, Xie Y, Xu Y, Hu J, Dai M. 2016. Physical-Biological Coupling in the Western South China Sea: The Response of Phytoplankton Community to a Mesoscale Cyclonic Eddy. PLoS One 11:e0153735.

Wang L, Huang B, Laws EA, Zhou K, Liu X, Xie Y, Dai M. 2018. Anticyclonic Eddy Edge Effects on Phytoplankton Communities and Particle Export in the Northern South China Sea. Journal of Geophysical Research: Oceans 123:7632-7650.

Ward BA, Dutkiewicz S, Jahn O, Follows MJ. 2012. A size-structured food-web model for the global ocean. Limnology and Oceanography 57:1877-1891.

Wong GTF, Tseng C-M, Wen L-S, Chung S-W. 2007. Nutrient dynamics and N-anomaly at the SEATS station. Deep Sea Research Part II: Topical Studies in Oceanography 54:1528-1545.

Xing X, Qiu G, Boss E, Wang H. 2019. Temporal and Vertical Variations of Particulate and Dissolved Optical Properties in the South China Sea. Journal of Geophysical Research: Oceans 124.

Xiu P, Chai F. 2011. Modeled biogeochemical responses to mesoscale eddies in the South China Sea. Journal of Geophysical Research 116.

Xiu P, Chai F, Shi L, Xue H, Chao Y. 2010. A census of eddy activities in the South China Sea during 1993–2007. Journal of Geophysical Research 115.

Xu W, Wang G, Cheng X, Jiang L, Zhou W, Cao W. 2022. Characteristics of subsurface chlorophyll maxima during the boreal summer in the South China Sea with respect to environmental properties. Sci Total Environ 820:153243.

Yasunaka S, Ono T, Sasaoka K, Sato K. 2022. Global distribution and variability of subsurface

Mesoscale eddy modulation of subsurface chlorophyll maximum layers in the South China Sea

chlorophyll a concentrations. Ocean Sci. 18:255-268.

Zhan P, Krokos G, Guo D, Hoteit I. 2019. Three‐Dimensional Signature of the Red Sea Eddies and Eddy‐Induced Transport. Geophysical Research Letters 46:2167-2177.

Zhang W-Z, Wang H, Chai F, Qiu G. 2016a. Physical drivers of chlorophyll variability in the open South China Sea. Journal of Geophysical Research: Oceans.

Zhang Z, Tian J, Qiu B, Zhao W, Chang P, Wu D, Wan X. 2016b. Observed 3D Structure, Generation, and Dissipation of Oceanic Mesoscale Eddies in the South China Sea. Sci Rep 6:24349.

# Figures and Tables
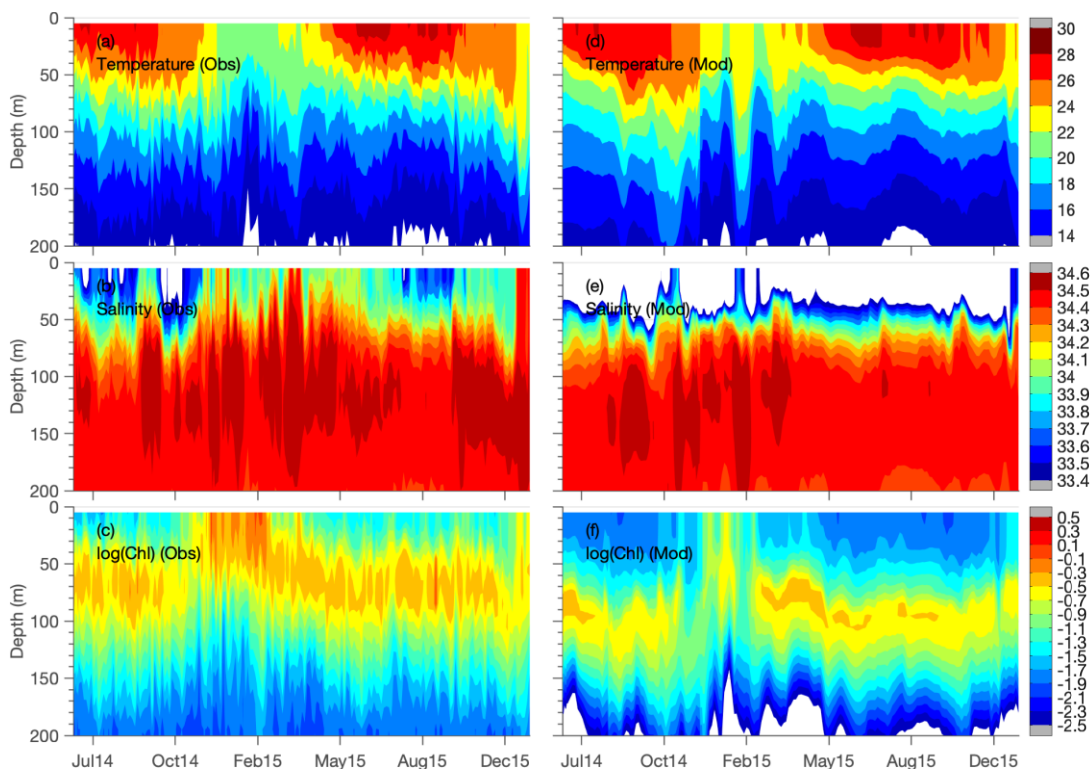


**Figure 1.** Observed (Obs) and simulated (Mod) variations of (a, d) temperature, (b, e) salinity and (c, f) chlorophyll-a with depth and time along the trajectories of the biogeochemical Argo floats in the northern South China Sea between July 2014 and December 2015. Observations presented in (a)–(c) have been modified from the results published in Xing et al. (2019).
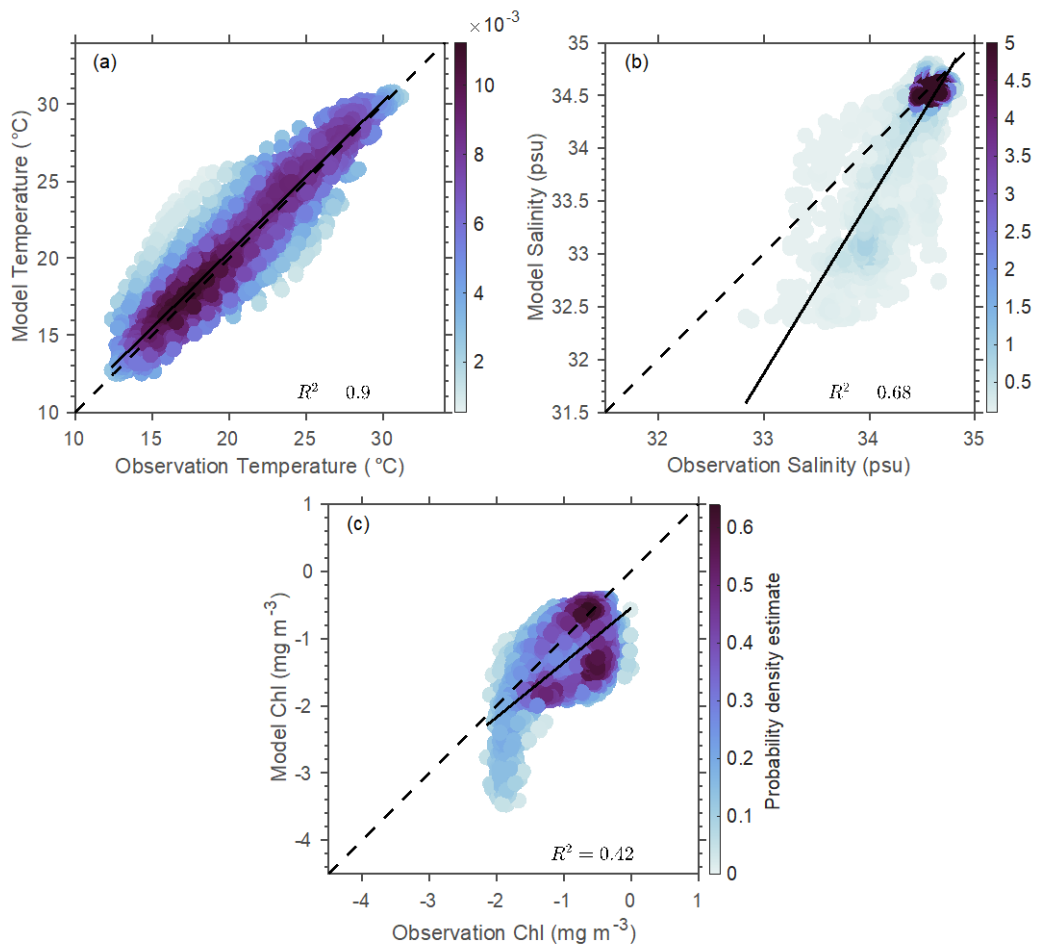
**Figure 2**. (a) Temperature, (b) salinity and (c) chlorophyll simulated by model

(Model) and measured by biogeochemical Argo floats (Observation). Color indicates

the density of the data. The dashed black line is the one-to-one line.
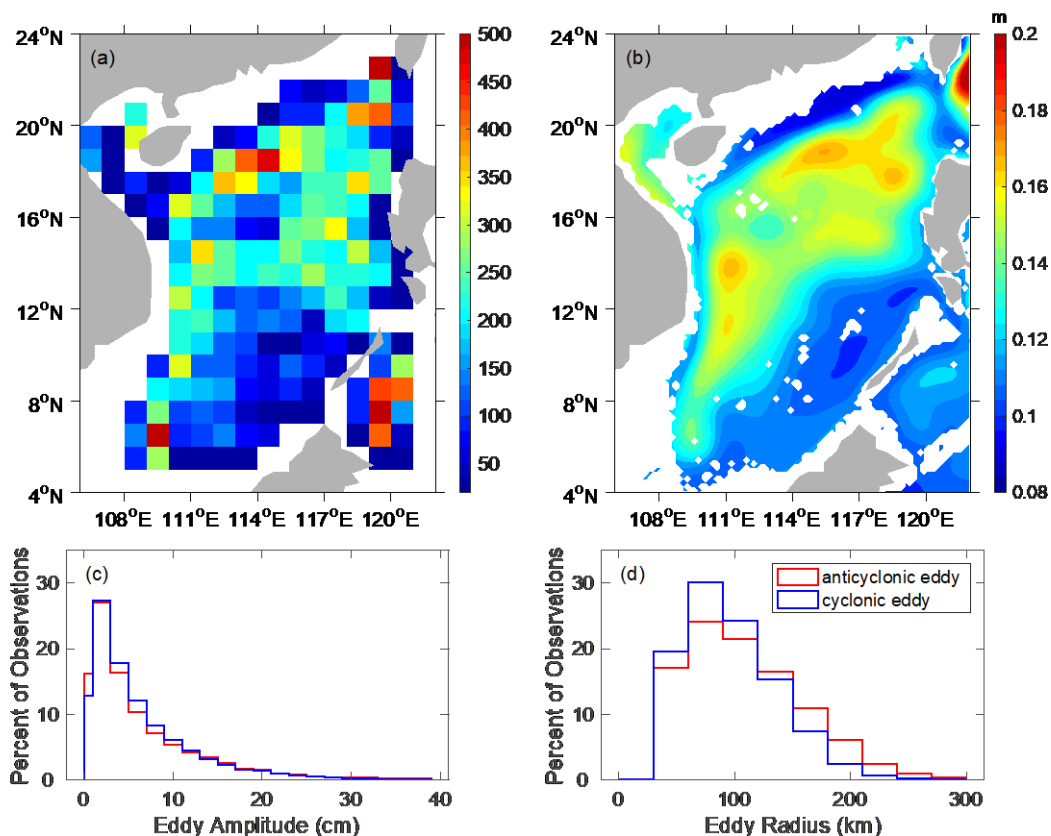
**Figure 3.** (a) Number of centroids of eddies (lifetime ≥ 30 days) passing through each 1° × 1° grid square over the study period of December 1993 to December 2015 (22 years). (b) Standard deviation of sea surface height based on 22-year model outputs. Histograms of (c) eddy amplitude and (d) mean eddy radius. In (c) and (d), only eddies with lifetime ≥ 30 days from the study period were included. The blue and red lines correspond to cyclonic and anticyclonic eddies, respectively.
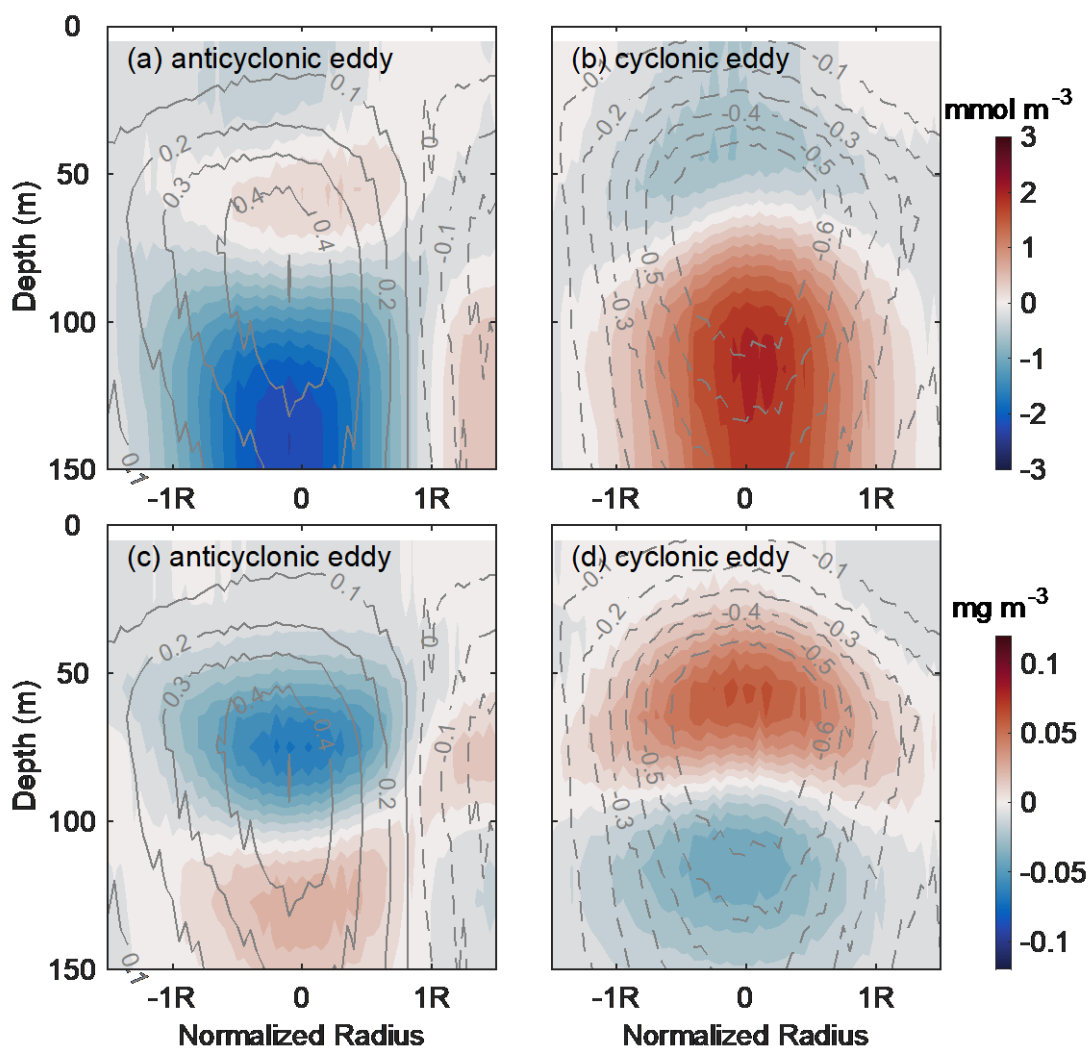
**Figure 4.** Composite zonal sections of vertical structure of (a, b) nutrient anomaly and (c,d) Chl anomaly across the anticyclonic eddy (left) and cyclonic eddy (right). Contours in each panel represent positive (solid lines) and negative (dashed lines) temperature anomaly at intervals of 0.1 °C.
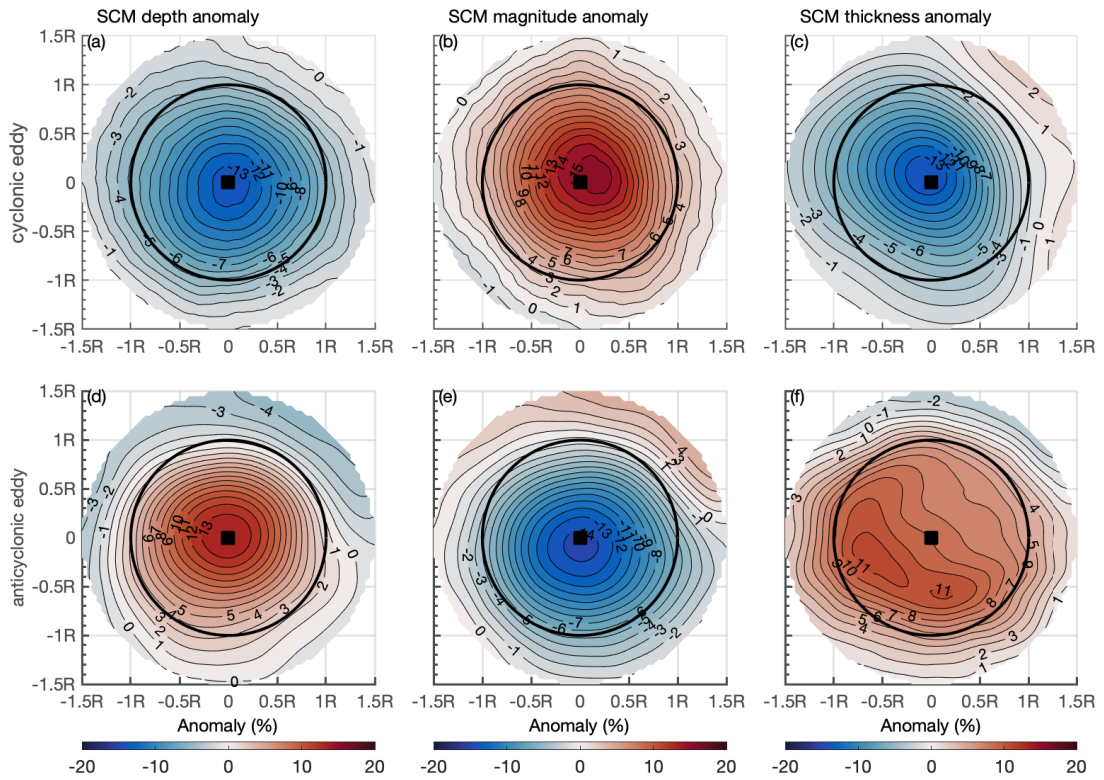
**Figure 5.** Composite maps of anomalies of subsurface chlorophyll maximum (SCM) depth, magnitude and thickness inside (a–c) cyclonic eddies and (d–f) anticyclonic eddies in the South China Sea. Axis values indicate the normalized distance between eddy center and eddy radius; R is the radius of the core of the eddy.
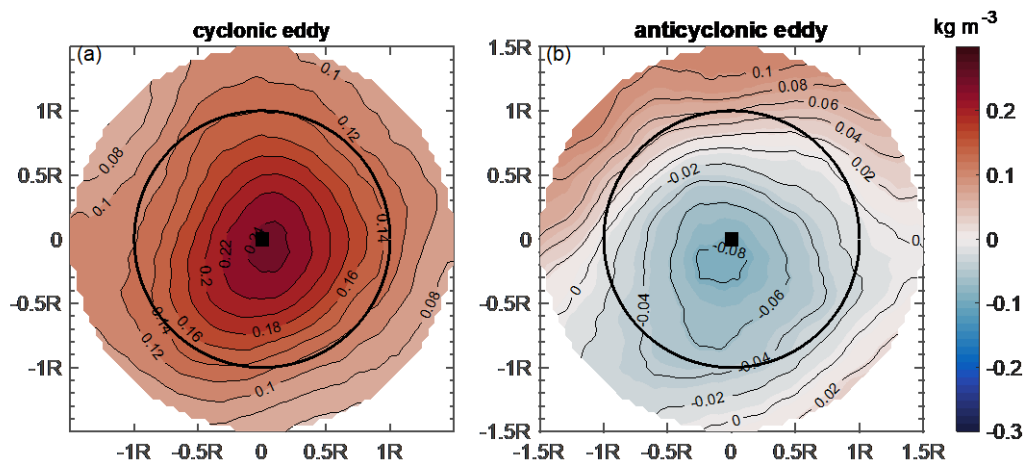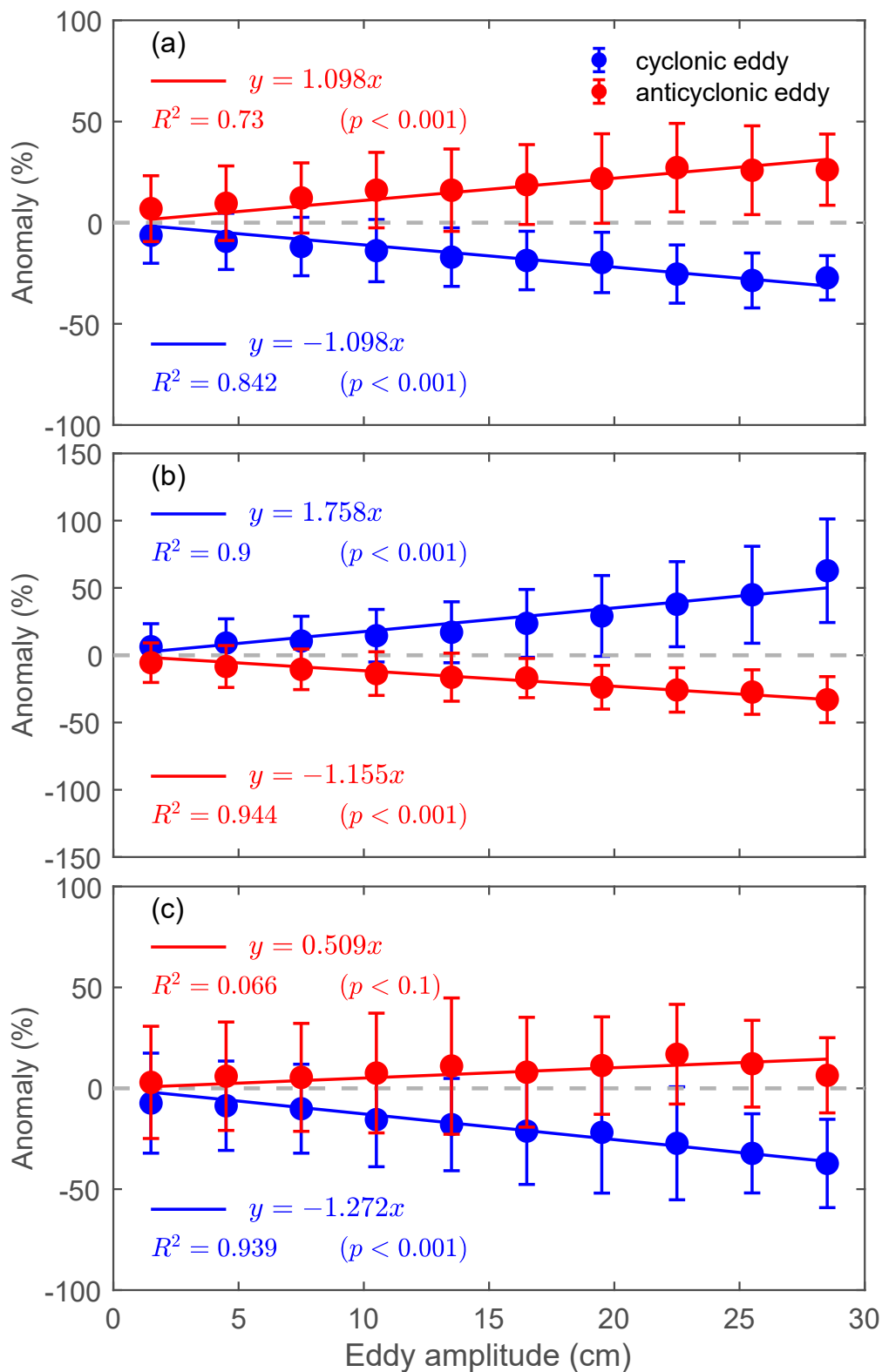
**Figure 6.** Composite maps of eddy-induced density anomalies in the subsurface chlorophyll maximum layer. Axis values indicate the normalized distance between eddy center and eddy radius; R is the radius of the core of the eddy.

**Figure 7.** Eddy amplitude and SCM (a) depth anomaly, (b) magnitude anomaly and (c) and thickness anomaly. The line represents the best linear fit result. The blue and red lines correspond to cyclonic and anticlonic eddies, respectively.
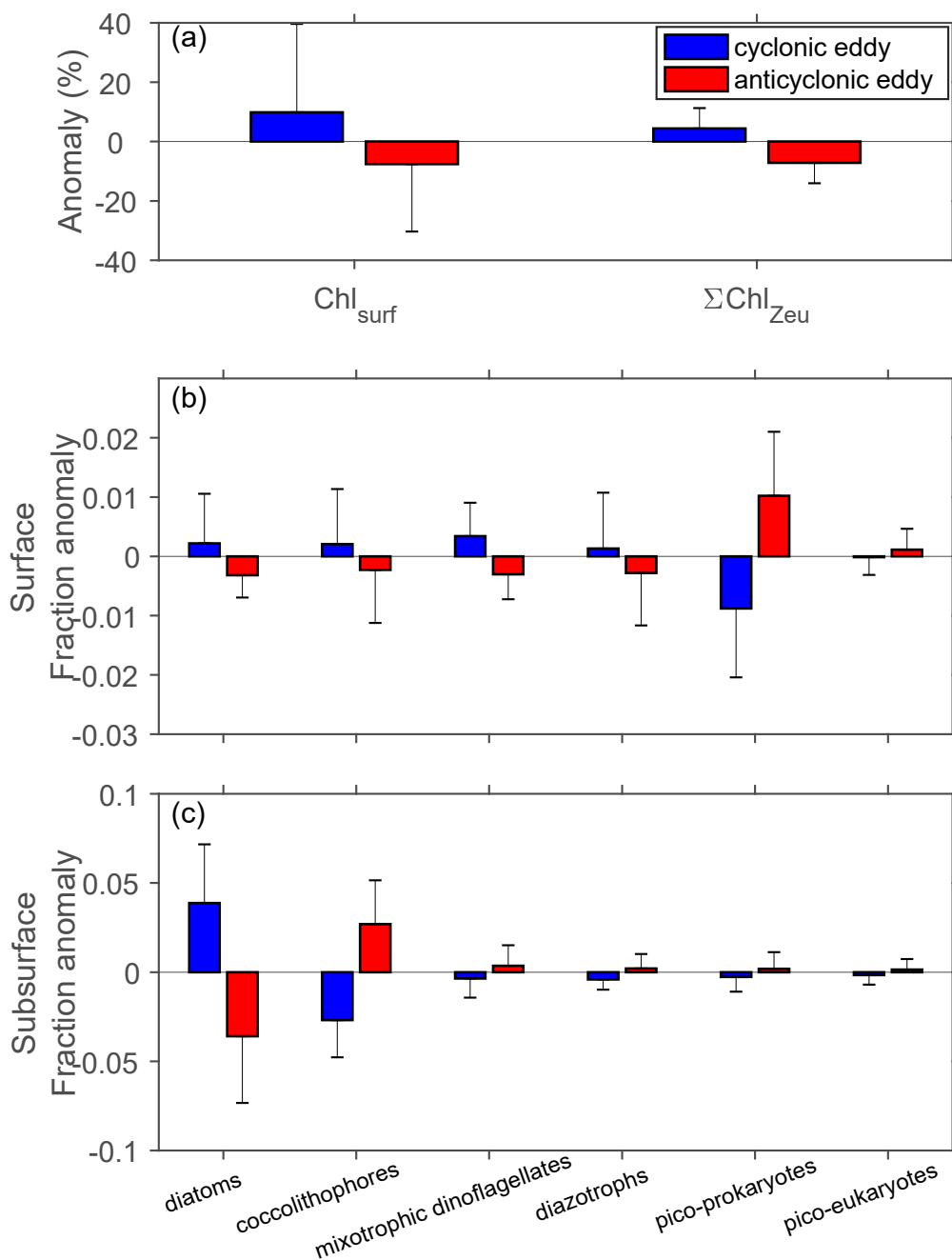
**Figure 8.** (a) Anomalies of eddy-induced surface chlorophyll (Chl$_{surf}$) and integrated chlorophyll in the euphotic layer ($\Sigma$Chl$_{Zeu}$). The fraction anomaly of phytoplankton function type in the (b) surface and (c) subsurface layers in the South China Sea. Error bar indicates the standard deviation of samples associated with each eddy center. Blue and red correspond to cyclonic and anticyclonic eddies, respectively.
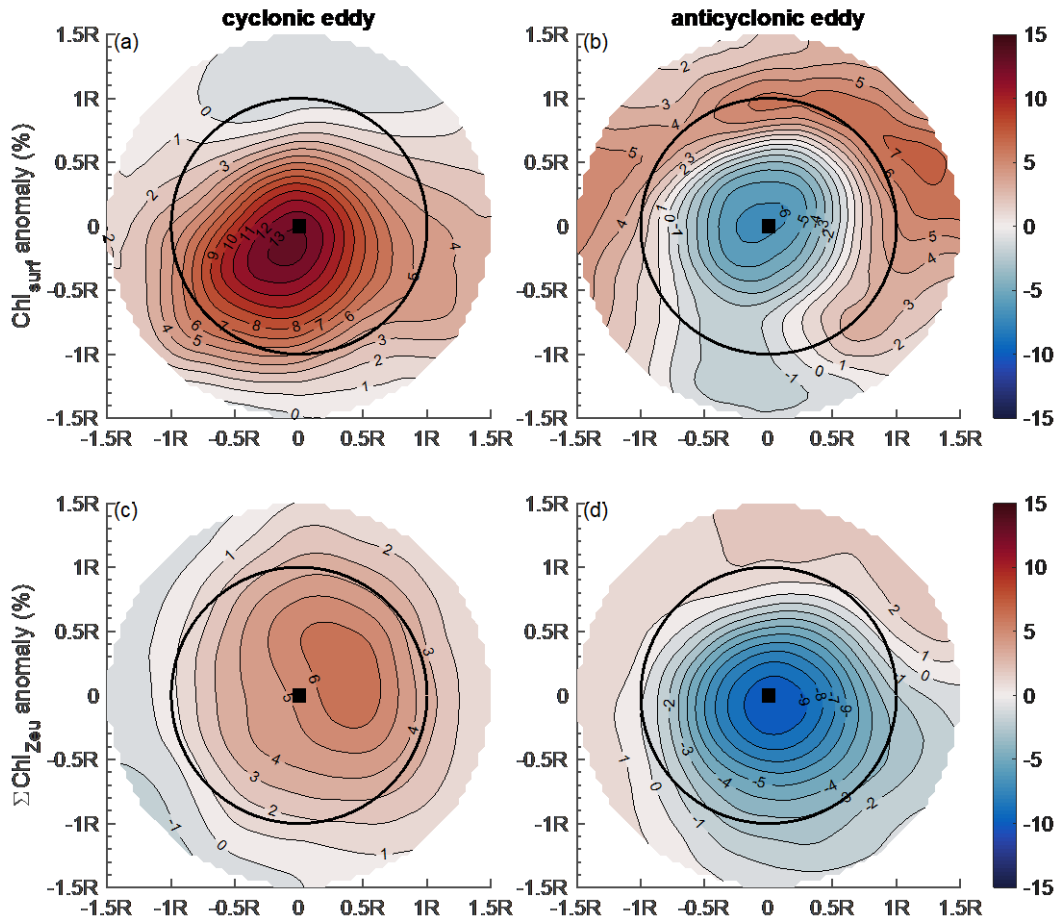
**Figure 9.** Composite maps of anomalies of (a, b) surface chlorophyll (Chl$_{surf}$) and (c, d) integrated chlorophyll between the surface and the euphotic depth (ΣChl$_{Zeu}$) in the South China Sea. Axis values indicate the normalized distance between eddy center and eddy radius; R is the radius of the core of the eddy.
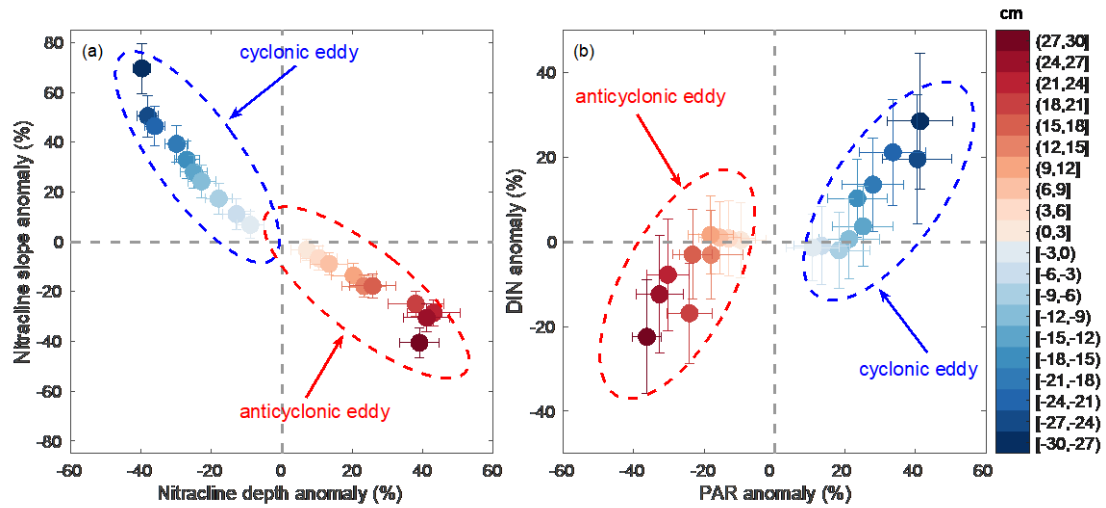
**Figure 10.** (a) Nitracline depth and slope anomalies and (b) dissolved inorganic nitrogen (DIN; sum of $NO_3^-$, $NO_2^{-2}$ and $NH_4^+$) and photosynthetically active radiation (PAR) anomalies in the subsurface chlorophyll maximum layer. Blue and red correspond to cyclonic and anticyclonic eddies, respectively. Color shades represent eddy amplitudes divided into 3-cm bins. Error bar represents the standard deviation of samples in each amplitude bin.
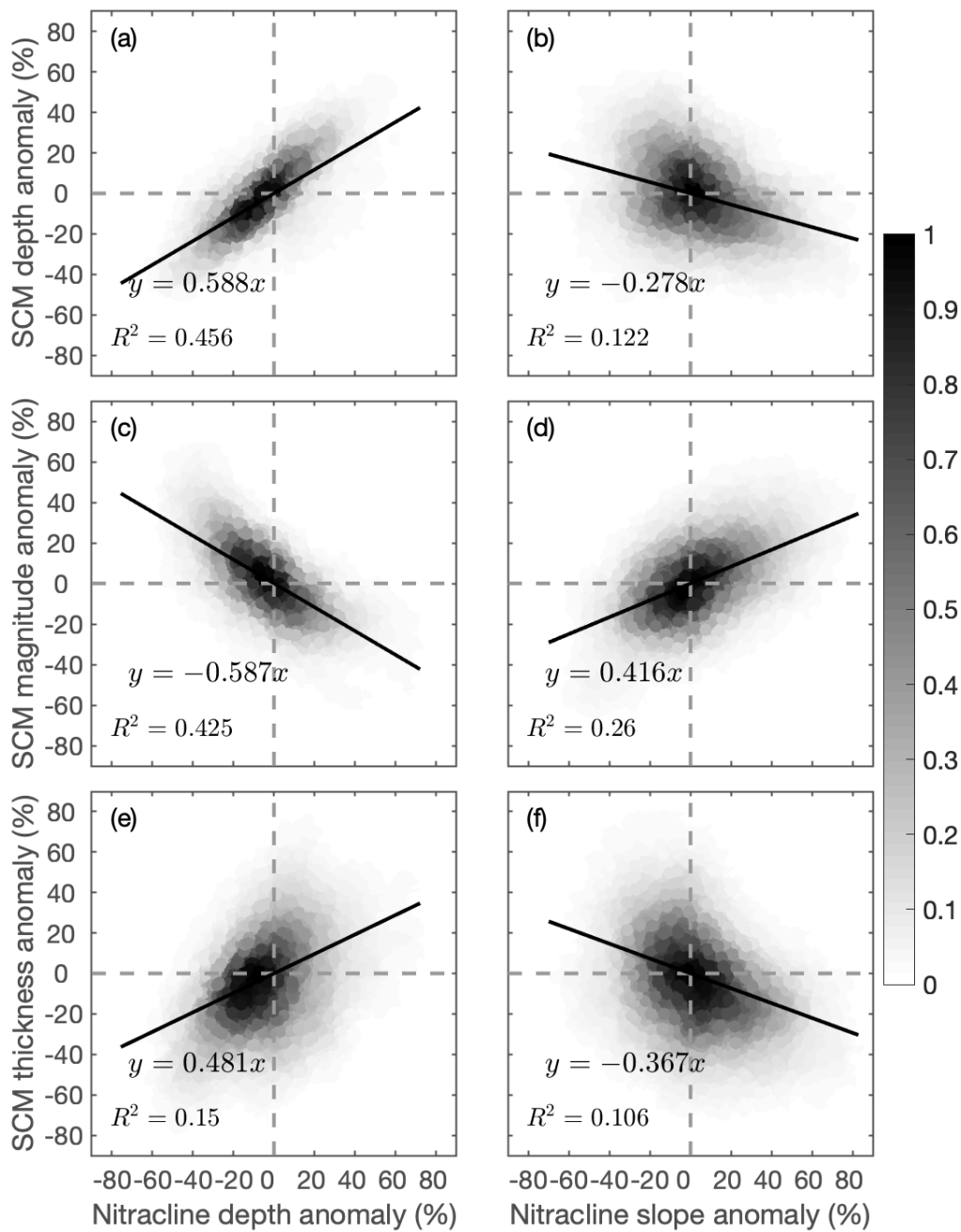
**Figure 11**. Scatter plots of nitracline depth and slope anomalies (x-axis) against SCM characteristic anomalies (y-axis). The black line represents the best linear fit result. Color indicates the density of the data.
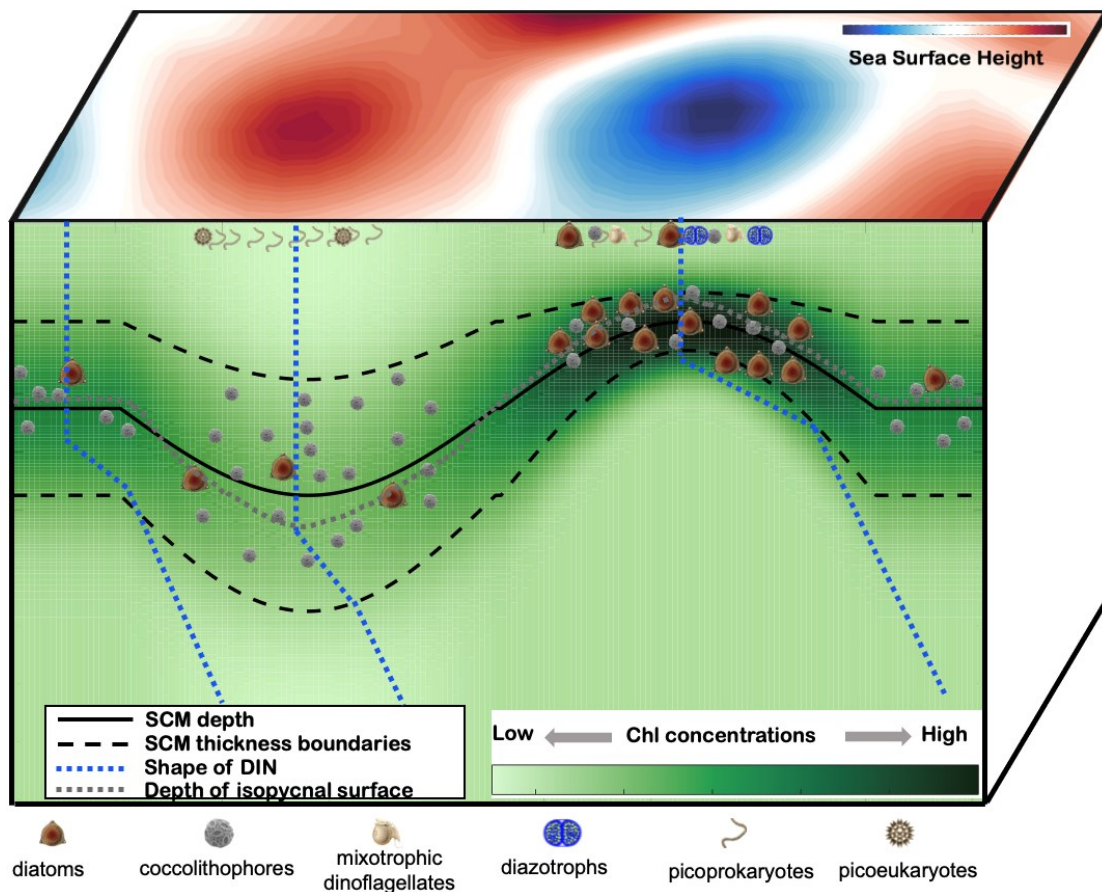
**Figure 12.** Schematic representation of mesoscale eddy modulation of the subsurface chlorophyll maximum layer in the South China Sea.

**Table 1.** Descriptive statistics of eddy characteristics.

| | Mean | Median | 25th percentile | 75th percentile | Minimum | Maximum |
|---|---|---|---|---|---|---|
| Amplitude AE (cm) | 6.9 | 4.6 | 2.3 | 9.3 | 1 | 40.8 |
| Amplitude CE (cm) | 7 | 4.9 | 2.5 | 9.4 | 1 | 40 |
| Radius AE (km) | 112.9 | 104.9 | 76.3 | 141.8 | 30.1 | 333 |
| Radius CE (km) | 99.1 | 92.1 | 69.9 | 122.6 | 30 | 289 |

Outliers with values of mean ± 5 standard deviations were excluded from the analysis. AE and CE stand for anticyclonic eddy and cyclonic eddy, respectively.